Processing and Application of Ceramics 16 [2] (2022) 143–152
https://doi.org/10.2298/PAC2202143P

High-density ceramics obtained by andesite basalt sintering

Vladimir Pavkov[1,*], Gordana Bakić[2], Vesna Maksimović[1], Ivana Cvijović-Alagić[1], Marija Prekajski Đorđević[1], Dušan Bučevac[1], Branko Matović[1]

[1]*Department of Materials Science, Vinča Institute of Nuclear Sciences - National Institute of the Republic of Serbia, University of Belgrade, Mike Petrovića Alasa 12-14, 11000 Belgrade, Serbia*
[2]*Faculty of Mechanical Engineering, University of Belgrade, Kraljice Marije 16, 11000 Belgrade, Serbia*

Received 8 September 2021; Received in revised form 11 February 2022; Accepted 12 April 2022

Abstract

In the present study, andesite basalt originated from the deposit site "Donje Jarinje", Serbia, was examined as a potential raw material for high-density ceramics production. The production of high-density ceramics included dry milling, homogenization, cold isostatic pressing and sintering in the air. To determine the optimal processing parameters the sintering was conducted at 1040, 1050, 1060, 1070 and 1080 °C, and afterwards the sintering duration was varied from 30 to 240 min at the optimal sintering temperature of 1060 °C. Characterization of the starting and sintered materials included the estimation of particle size distribution, density, hardness and fracture toughness complemented with X-ray diffraction, optical light microscopy, scanning electron microscopy and energy dispersive spectroscopy analysis. Phase transformations did not occur during processing in the investigated temperature range from 1040 to 1080 °C. The obtained research results showed that 99.5% of relative density and the highest hardness and fracture toughness values of 6.7 GPa and 2.2 MPa·m$^{1/2}$, respectively, were achieved for the andesite basalt sintered at 1060 °C for 60 min in the air. The results of the present study confirmed that the sintered andesite basalt can be used as a high-density ceramic material for various industrial applications.

Keywords: *andesite basalt, sintering, mechanical properties, optical microscopy, structural applications*

I. Introduction

In modern industrial practice, environmentally friendly and lightweight constructive materials with good mechanical properties, produced from low-cost abundant materials, are highly demanded. Basalt is a natural material that meets all of these criteria. Namely, basalt is a natural igneous rock of volcanic origin, which covers about 70% of the Earth's crust [1]. As a result of the rapid cooling of lava on the Earth's surface, basalt is usually present in fine-grained condition and belongs to the group of grey-to-black coloured and extremely hard rocks. The technology of basalt rock processing is entirely eco-friendly, which is extremely important for the modern age economy, ecology and energy-efficiency.

Basalt can be used in the production of heat- and fire-resistant refractory materials owing to its low thermal conductivity, high oxidation resistance and high softening and melting temperatures [2]. Because of the high chemical durability and high resistance to abrasion and corrosion [3–5], natural basalts are regarded as good replacements for wear-resistant steels and can be used for the production of constructive elements which are exposed to abrasion and corrosive-abrasive wear during their exploitation [6].

Since basalt shows no toxic, carcinogenic, mutagenic, or teratogenic effects [6] it is in a real sense non-hazardous material [7]. High strength, hardness and toughness [8], low viscosity [9], high corrosion resistance, minimal moisture absorption, ability to withstand high temperatures, thermal insulation and sound absorption properties [10,11], high abrasion resistance, exceptional compressive strength and chemical resistance resulted in the usage of basalt-based products in various industrial applications from civil and mechanical engineering, agriculture, construction industry and mining, to transportation industry, metallurgy [12–17] and as a decorative material [16,18].

Moreover, basalts can be used as raw materials for obtaining iron-rich glass and glass-ceramic materials

*Corresponding author: tel: +381 65 50 54 280
e-mail: *pavkow@vin.bg.ac.rs*

[19–24] due to their chemical composition since these volcanic rocks are mainly composed of silica, alumina, iron oxide, calcium oxide and magnesia with lower content of potassium, titania, manganese and phosphorus oxide [14]. Classification of basalt rocks is conducted according to the SiO_2 content present in their composition and thus basalts can be classified as alkaline (up to 42% SiO_2), mildly acidic (43–46% SiO_2) and acidic (over 46% SiO_2) [25].

Even though basalt shows numerous advantages for application in diverse industrial areas it is still mostly used in civil engineering, while research data regarding their wider applicability are scarce in the available literature. For this reason, the aim of the present research was to define the optimal technological procedure in order to obtain low-cost high-density ceramics based on basalt with advanced characteristics and to evaluate their potential industrial applications as environmentally friendly materials. Furthermore, the high-density ceramics can be used as a matrix in the production of advanced composite materials with improved physical and mechanical properties in comparison to monolithic basalt.

II. Experimental

2.1. Materials and synthesis

Crushed basalt aggregates 2 to 5 mm in size, supplied from the deposit site "Donje Jarinje", Serbia, were used as a starting material. The basalt from this deposit site is distinctly black coloured and textured, classified as the andesite basalt [6,17], also mentioned in the literature as the basaltic andesite [26].

The chemical composition of the andesite basalt used in this study was analysed utilizing the Oxford INCA 350 energy dispersive X-ray (EDX) microanalysis system (Oxford Instruments, UK) coupled with the JEOL JSM-6610LV scanning electron microscope (SEM, JEOL, Japan). For this purpose, five andesite basalt samples were examined and obtained results are summarized in Table 1. The obtained results indicate that the determined chemical composition is characteristic for the andesite basalt rock, i.e. content of silica and alumina oxides as predominating compounds in the rock composition is approximately 77 wt.%. Based on the determined SiO_2 content of approximately 58 wt.% (Table 1), the basalt rock, used in this study, can be classified as acidic.

The andesite basalt was milled in a tungsten-carbide vibrating cup mill Fritsch Pulverisette 9, Germany, for 30 min in a dry state at 800 rpm to obtain the fine powder suitable for synthesis. The obtained powder was mixed with 0.6 wt.% of commercial paraffin wax binder for 10 min in a ceramic mortar. After homogenization, the powder mixture was preloaded under a cold uniaxial pressure of 50 MPa to obtain cylindrical green compacts 12 mm in diameter and afterwards subjected to the cold isostatic pressing (CIP) under a pressure of 230 MPa for 2 min to increase the green compacts density. To remove the binder, organic impurities, moisture and chemically bonded water, the green compacts were slowly heated up in the air to 100 °C at the heating rate of 1 °C/min and held at this temperature for 60 min, and then additionally heated with the same rate to 650 °C and held for 60 min. After binder removal, the basalt-based compacts were heated to the chosen sintering temperature with the heating rate of 5 °C/min.

The basalt-based compacts were sintered in the air in the laboratory high-temperature electric resistance box furnace Elektron VTP-03, Serbia, for 60 min at 1040, 1050, 1060, 1070 and 1080 °C to determine the optimal sintering temperature necessary for the attainment of the ceramic materials with the highest density. The sintering temperature was constantly monitored and electronically regulated within the maximal temperature deviation of ±2 °C. The cooling rate from sintering to room temperature was 5 °C/min. After determining the optimal sintering temperature, additional group of samples was sintered at the optimal temperature for 30, 60, 120, 180 and 240 min to determine the optimal sintering duration.

2.2. Materials characterization

Laser particle size analyser Mastersizer 2000, Malvern Instruments Ltd., UK, was utilized to determine the particle size distribution of the milled andesite basalt powder. Pycnometric density of the andesite basalt powder was measured using a pycnome-

Table 1. The chemical composition of the andesite basalt originated from the "Donje Jarinje" deposit site

Compounds	Chemical composition [%]				
	Sample 1	Sample 2	Sample 3	Sample 4	Sample 5
SiO_2	58.21	57.76	59.98	58.97	58.21
Al_2O_3	18.97	19.96	18.34	19.27	18.19
FeO	6.66	5.54	7.36	6.19	7.08
CaO	5.63	7.14	6.91	6.45	7.68
Na_2O	3.94	3.40	2.68	2.47	2.25
MgO	2.86	3.32	1.50	3.57	3.51
K_2O	2.79	2.24	2.61	2.19	2.18
TiO_2	0.95	0.65	0.62	0.87	0.89
Total	100.00	100.00	100.00	100.00	100.00

ter, distilled water and analytical balance KERN PFB, Germany, with an accuracy of ±0.01 g. Density of the sintered ceramic samples was determined by employing the Archimedes' principle using distilled water as the immersion liquid. Relative density of the obtained ceramics was calculated based on the theoretical density (TD). All density measurements were conducted for 5 samples and showed excellent reproducibility.

Phase analysis of the milled andesite basalt powder and sintered ceramic samples was conducted by using X-ray diffractometer (XRD, Rigaku Ultima IV, Japan), with filtered Cu$K\alpha_1$ radiation ($\lambda = 0.154178$ nm). X-ray diffraction data were collected over the 2θ range from 3° up to 70° with the step of 0.02° and scanning rate of 5 °/min. The PDXL2 v2.0.3.0 software with reference to the diffraction patterns available in the International Center for Diffraction Data (ICDD) was used for the phase identification and data analysis.

To examine the microstructural and morphological characteristics, the sintered ceramic samples were ceramographically prepared using the standard preparation method that included grinding with SiC abrasive papers up to 1000 grit and polishing using 1 μm diamond paste. The microstructure of the sintered samples was investigated by a optical light microscope (LOM) Zeiss Axioplan LM, Zeiss, Germany. Morphological characterization of the andesite basalt powder and sintered ceramic samples was performed using an SEM Tescan VEGA TS 5130 MM, Tescan, Czech Republic.

The sintered samples hardness and fracture toughness were determined utilizing the Vickers indentation hardness tester model Buehler Identamet 1114, Buehler, Germany, by applying a load of 3 kgf (29.421 N). All Vickers hardness measurements were conducted at 5 measuring points on each sample with excellent reproducibility. The Vickers hardness (HV) was calculated according to Eq. 1 [27]:

$$HV = 1.854 \cdot 10^{-9} \frac{P}{d^2} \quad (1)$$

where P is an indentation load, while d is an average length of the diagonals of the Vickers indentation. The half-penny crack model [28] was used for the calculation of the fracture toughness in brittle materials according to Eq. 2:

$$K_{IC} = 0.0752 \frac{P}{c^{3/2}} \quad (2)$$

where K_{IC} is the fracture toughness, P is the indentation load, while c is the measured crack length. If a is the half-diameter of the indented section and $c/a \geq 2$ then the crack model can be considered as a half-penny model, while if $c/a < 2$ then the crack model is considered as the Palmqvist model [29,30]. The general assumption is that cracks in brittle materials, characterized with relatively low toughness, are following the half-penny model and that cracks attained in materials with relatively high toughness can be considered to emulate the Palmquist model [31].

III. Results and discussion

3.1. Powder characterization

Pycnometric density of the milled andesite basalt powder was determined to be 2.63 g/cm^3. This is in a good agreement with the available literature data showing that density of the andesite basalt originated from the "Donje Jarinje" deposit site is in the range from 2.60 to 2.63 g/cm^3 [6,17].

Particle size distribution of the andesite basalt powder obtained by milling the basalt rock is shown in Fig. 1. As it can be seen, the values obtained during the powder analysis can be summarized as follows: $d_{10} = 0.465$ μm, $d_{50} = 1.917$ μm and $d_{90} = 11.803$ μm. Bimodal distribution of the powder particles size is evident in the range from 0.2 to 12 μm and from 100 to 300 μm. The volume fraction of powder particles with dimensions ranging from 0.2 to 12 μm is determined to be 93.3%, while the volume fraction of powder particles with dimensions ranging from 100 to 300 μm is estimated to be 6.7%. The observed bimodal particle size distribution enables good powder compaction with the usage of a minimal amount of binder.

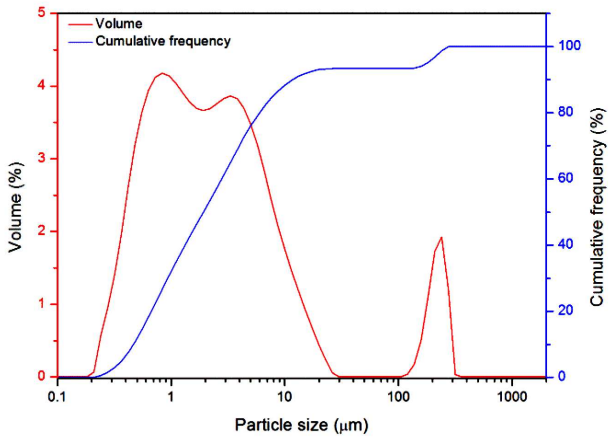

Figure 1. Particle size distribution of the andesite basalt powder obtained after dry milling for 30 min

The morphology of the andesite basalt powder obtained by dry milling for 30 min is presented in Fig. 2. The presence of angularly shaped particles with a rough surface is clearly visible in the SEM micrograph. Moreover, agglomeration of small powder particles of approximately 0.5 μm in size can also be observed in Fig. 2.

Phase analysis of the starting andesite basalt material was performed using X-ray powder diffraction analysis to reveal its main mineralogical composition. For that purpose, the andesite basalt rock was crushed and milled into fine powder form. The obtained andesite basalt mineralogical composition is presented in Fig. 3. Based on XRD analyses, andesine, as an intermediate member of plagioclase mineral series ((Na,Ca)Al(Si,Al)Si_2O_8), was identified as a dominant mineral of the basalt rock used in the present re-

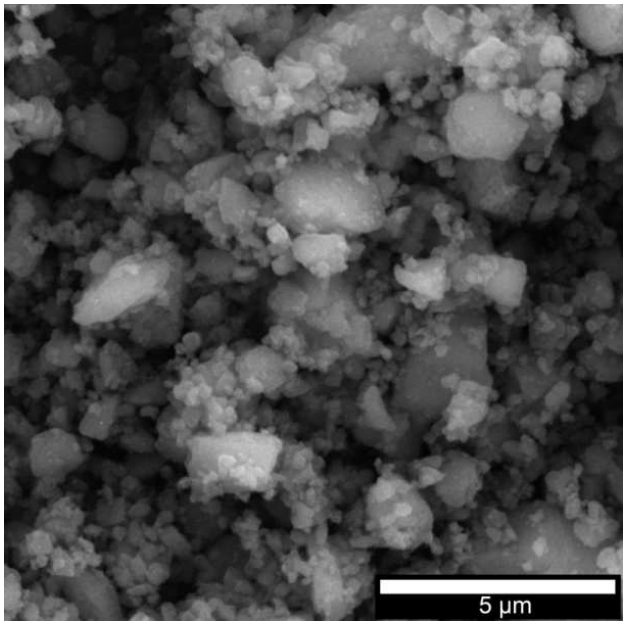

Figure 2. SEM micrograph of the andesite basalt powder obtained after dry milling for 30 min

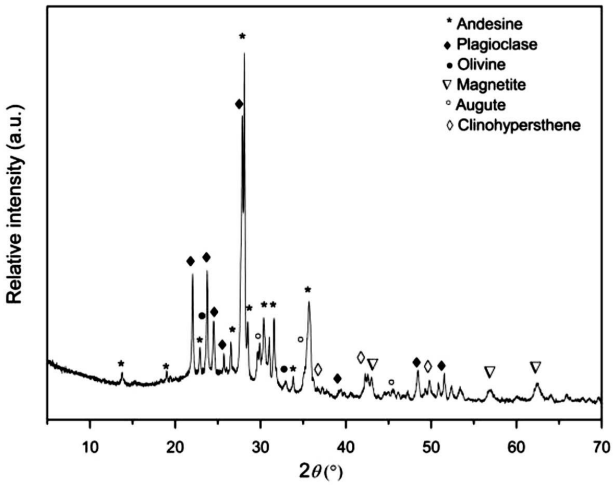

Figure 3. XRD pattern of the starting andesite basalt powder

search. Moreover, labradorite ((Ca,Na)Al(Al,Si)Si_2O_8), as another mineral from the plagioclase series which is richer in Ca than andesine, was also identified. Furthermore, small amounts of other minerals, such as olivine ($(Mg,Fe)_2SiO_4$) and magnetite (Fe_3O_4), as well as the common rock-forming pyroxene minerals, such as augite ((Ca,Na)(Mg,Fe,Al,Ti)$(Si,Al)_2O_6$) and clinohyperstene ((Mg,Fe)SiO_3), were additionally identified in the basalt rock sample.

3.2. Characterization of sintered samples

XRD patterns of all sintered high-density ceramic samples obtained during the present study along with starting andesite basalt powder are presented in Fig. 4. Since the sintered ceramic samples are pressed in the form of a pastille they had to be placed in a sample holder for the solid sample analysis. This holder is made

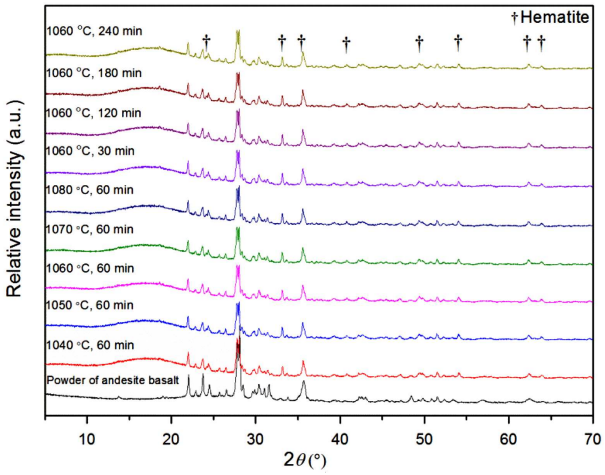

Figure 4. XRD patterns of the andesite basalt powder and ceramic samples attained during sintering under different sintering conditions

of polyethylene terephthalate glycol (PETG) by using the Ender-5 3D printer, Creality, China. Due to the usage of the PETG sample holder, small intensity hump (broad peak) in the low angle region (2θ range from 10° to 20°) can be observed on the recorded XRD patterns, indicating the presence of amorphous phase ascribed to PETG.

Detailed analysis of the obtained XRD patterns, given in Fig. 4, shows that there is no significant difference between the recorded diffractograms of the ceramic samples sintered under different conditions indicating the absence of the phase transformations during these treatments. The only difference that can be singled out is the presence of haematite (Fe_2O_3) in the patterns of the high-density ceramic samples which is absent in the XRD pattern of the starting andesite basalt powder. The appearance of haematite during sintering in air was expected (see Eq. 3) and the assumption on the transition from FeO to Fe_2O_3, which was based on the colouration of the sintered samples, is in this way confirmed.

It can be observed that the initial black colour of the andesite basalt rock is transformed after milling into the grey colour of the obtained basalt powder which is additionally transformed during sintering in air to the reddish-brown colour of the ceramic samples. The observed colour change is induced by the chemical composition alterations, i.e. the transition of FeO into Fe_2O_3 according to the following equation:

$$4\,FeO + O_2 \longrightarrow 3\,Fe_2O_3 \qquad (3)$$

The final surfaces of the sintered samples under an oxidizing atmosphere have reddish-brown colour suggesting the presence of Fe^{3+} ions and the formation of haematite (Fe_2O_3) [32–36].

The effect of sintering temperature on density of the ceramic samples obtained after sintering for 60 min is presented in Fig. 5. As it can be seen, the lowest relative density of 92.9% was measured in the ceramic samples

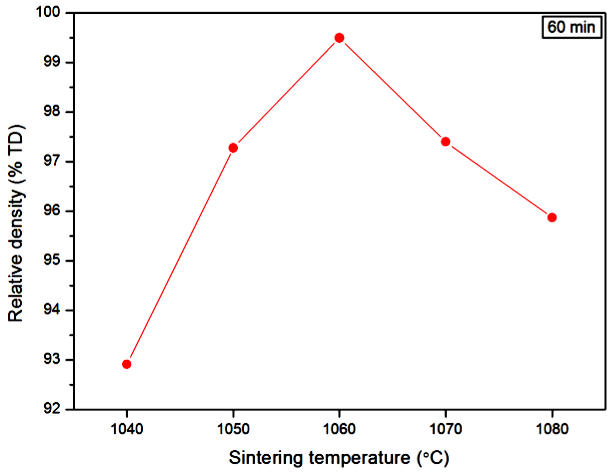

Figure 5. Effect of sintering temperature on the density of ceramic samples obtained during sintering for 60 min

sintered at 1040 °C. The relative density of the obtained ceramics increases with an increase in sintering temperature reaching the maximum value of 99.5% in the sample sintered at 1060 °C. Therefore, this temperature was designated as optimal. Based on the available literature data [17,36,37] and results obtained in the present study, this is the highest relative density achieved during basalt sintering. With the further increase of sintering temperature, relative density of the obtained ceramic samples decreases. Namely, at sintering temperature of 1080 °C relative density of 95.8% is achieved. Research results presented in Fig. 5 show that small sintering temperature alterations have a significant impact on relative density.

It is believed that relatively low density of the samples sintered at 1080 °C is the result of melting of glassy phase which is normally present in basalt. It is well known that the presence of liquid phase can promote densification by activating so called liquid phase sintering mechanism. However, if sintering temperature is too high the effect of liquid phase presence is completely opposite. The increased vapour pressure leads to filling of the pores with gas which suppresses their elimination during sintering. Therefore, porosity of the sample sintered at 1080 °C was quite high reaching value of 4.2% (Fig. 5).

The decrease in density of the samples sintered above 1060 °C can be explained with the help of "liquid channels". In the localized surface area of the ceramic samples sintered at 1070 and 1080 °C the appearance of so-called "liquid channels" was noticed. The similar phenomenon was observed at the andesite basalt surface originated from the same location [17]. This phenomenon was also reported for the olivine basalt as well as some other similar materials and explained with the occurrence of partial melting of formed crystal phases between the solidus and liquidus temperatures [37,38]. Moreover, previous research in this field showed that a higher silicon, sodium and potassium contents in the basalt composition led to an increase of the glassy phase content in the microstructure, which reduced the material density and increased its acid resistance [39].

Polished surfaces of the ceramic samples sintered at 1040, 1060 and 1080 °C for 60 min are presented in Fig. 6. Shown LOM micrographs demonstrate that the reason for a decrease in the relative density of the samples sintered above 1060 °C is the appearance of surface craters as a result of melting and evaporation of the material, Fig. 6c. Size of the observed surface craters is up to 50 μm.

The effect of sintering time on density of the ceramic samples sintered at 1060 °C is presented in Fig. 7. A decrease of sintering duration from 60 to 30 min, as well as an increase of the sintering time to 120, 180 and 240 min, did not lead to an increase of relative density. Namely, the obtained results indicated that the relative density of the sintered samples decreased with an increase in sintering time. Therefore, the optimal sintering temperature and time were found to be 1060 °C and 60 min, respectively.

The effect of sintering parameters on the shrinkage of the high-density ceramic samples is presented in Fig. 8. The effect of sintering temperature on shrinkage is given in Fig. 8a which shows that the shrinkage increases with an increase in sintering temperature, reaching the maximum value of 12.81% in the samples sintered at 1060 °C. Further increase in sintering temperature causes a decrease of shrinkage reaching the value of 10.83% in the samples sintered at 1080 °C.

The difference between the maximum and minimum shrinkage value of 1.98% was observed during the sintering in the specified temperature range. If graphs given in Figs. 5 and 8a are compared, one can conclude that

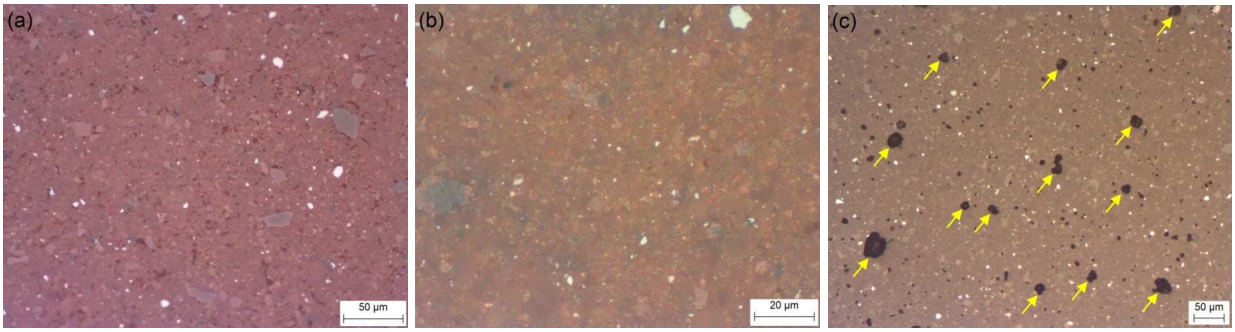

Figure 6. LOM micrographs of the high-density ceramic samples sintered at: a) 1040 °C, b) 1060 °C and c) 1080 °C for 60 min

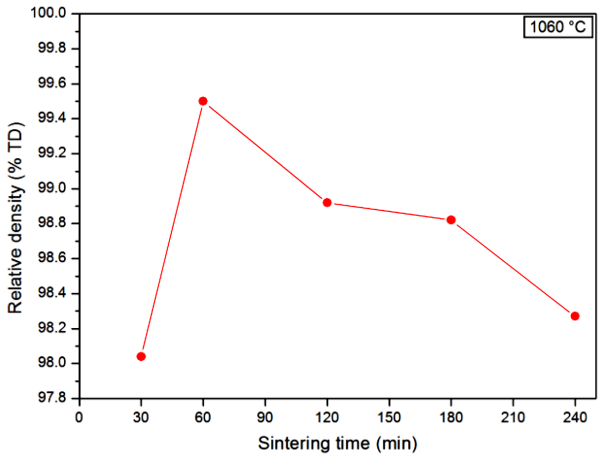

Figure 7. Effect of sintering time on the density of samples obtained after sintering of the andesite basalt powder at 1060 °C

the effect of sintering temperature on relative density and shrinkage is quite similar. This is expected knowing that the increase of relative density as well as the increase of shrinkage is affected by pore elimination.

The effect of sintering time on the shrinkage of high-density ceramic samples sintered at 1060 °C is presented in Fig. 8b. It is evident that a decrease in sintering time to 30 min, as well as an increase in sintering time to 120, 180 and 240 min, did not contribute to an increase of the shrinkage. The lowest shrinkage of 12.12% was measured in the samples sintered for 240 min. The negligible difference of only 0.69% between the maximum and minimum shrinkage value could be detected at the optimal sintering temperature.

The effect of sintering parameters on weight loss of the obtained high-density ceramic samples is presented in Fig. 9. From the research results presented in Fig. 9a, it can be observed that the highest weight loss of 3.10 wt.% was detected during sintering at 1080 °C, while the lowest weight loss of 2.81 wt.% was measured after sintering at 1050 °C. The slight difference between the maximum and minimum weight loss value of 0.29 wt.% was observed during the high-density ceramics sintering in the specified temperature range, although the detected weight loss was increased with an increase of sintering temperature to 1080 °C.

The effect of sintering duration on the weight loss of high-density ceramic samples attained during sintering of the andesite basalt powder at 1060 °C is presented in

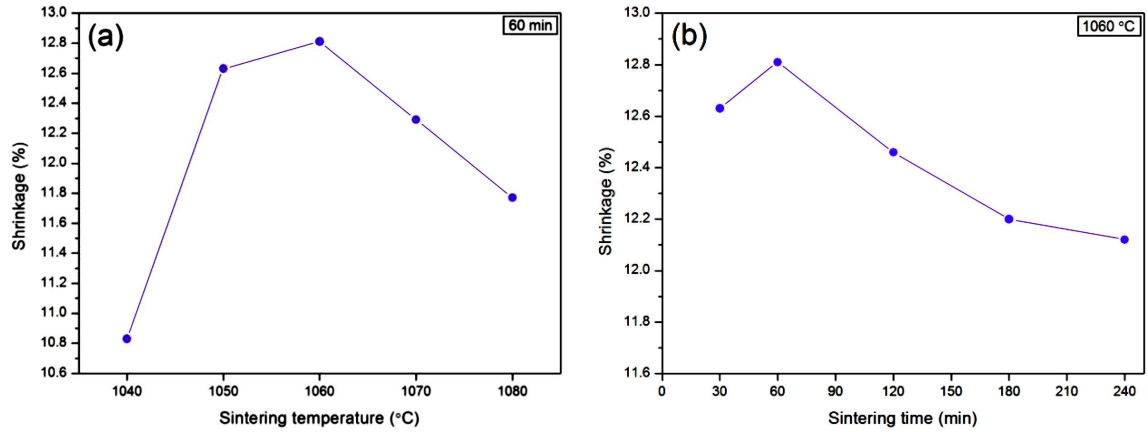

Figure 8. Shrinkage during sintering of the andesite basalt powder at: a) different temperatures for 60 min and b) 1060 °C for different sintering time

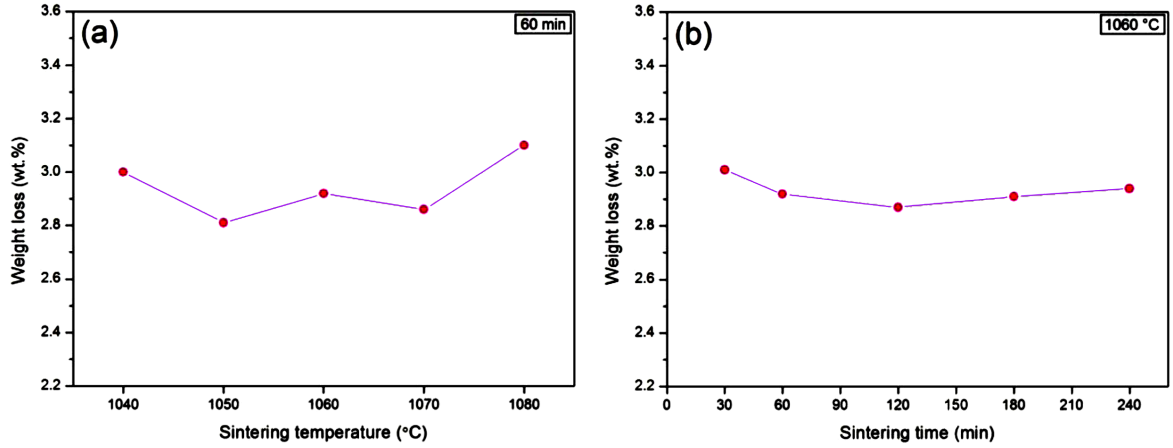

Figure 9. Weight loss during sintering of the andesite basalt powder at: a) different temperatures for 60 min and b) 1060 °C for different sintering time

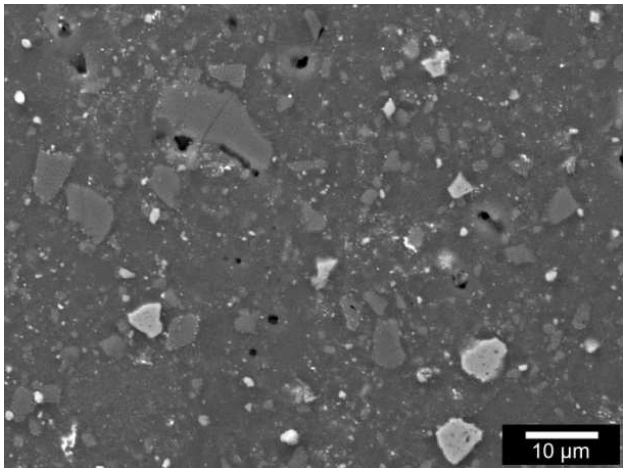

Figure 10. SEM micrograph of the ceramic sample attained during sintering of the andesite basalt powder at 1060 °C for 60 min

Fig. 9b. Presented results indicate that during the processing at the optimal sintering temperature in the sintering time range from 30 to 240 min, the highest weight loss of 3.01 wt.% was evident after sintering for 30 min, while the lowest weight loss of 2.87 wt.% was shown for the ceramic samples sintered for 120 min. Namely, the negligible difference of only 0.14 wt.% between the maximum and minimum weight loss value could be detected after the high-density ceramics sintering at the optimal sintering temperature.

It must be emphasized that the weight loss in the range from 3.19 to 3.77 wt.% was also recorded during the sintering of the basalt originated from the Arkhangelsk region in Russia where the detected weight change variation was confirmed to be within 0.60 wt.% range [39]. Having this in mind, it can be concluded that the lower weight loss was recorded during the sintering in air of the andesite basalt originated from the deposit site "Donje Jarinje", which was used in this study, than during the sintering of the basalt from the deposit site located in the Arkhangelsk region, which was reported in the literature. Previously published results indicate that during the basalt heat treatment, the weight loss can be expected due to the hygroscopic moisture evaporation, the chemically bound water removal, burnout of the organic impurities, dissociation of the present carbonates and sulphides and removal of the gaseous inclusions [36,39]. Therefore, it can be presumed that the andesite basalt from the "Donje Jarinje" deposit site shows higher purity and can be considered as a high-quality raw material for the high-density ceramics production.

SEM micrograph of the polished surface of the high-density ceramic sample obtained after sintering at 1060 °C for 60 min is given in Fig. 10. Isolated closed spherically-shaped pores, with dimensions up to 2 µm, are visible after sintering under these optimized conditions (Fig. 10) in contrast to the distinctly irregularly-shaped pores with mostly negative curvatures and a large surface-to-volume ratio present in the ceramic sample obtained during sintering at 1040 °C for 60 min (Fig. 6a). Namely, it can be concluded that with an increase of sintering temperature, pores inevitably present in the ceramic structure will tend to change their shape, i.e. pores will tend toward cylindrical to spherical morphologies and positive curvature with the lowest surface-to-volume ratio, clearly visible in Fig. 10. SEM micrograph, shown in Fig. 10, also indicates the non-homogeneous structure of the ceramic sample obtained during sintering at 1060 °C for 60 min in the presence of different aggregates and a clear boundary in between.

3.3. Mechanical properties

The effect of sintering temperature on the hardness of the ceramic samples attained during sintering of the andesite basalt powder for 60 min is presented in Fig. 11a. A minimal hardness value of 4.8 GPa was achieved at an initial sintering temperature of 1040 °C. With the increase of sintering temperature, the hardness increases and reaches a maximal value of 6.7 GPa after sintering at 1060 °C. With a further increase in sintering temperature, the hardness value begins slightly to decrease and for the ceramic sample obtained at 1080 °C the hardness value reaches 6.1 GPa. By comparing the obtained den-

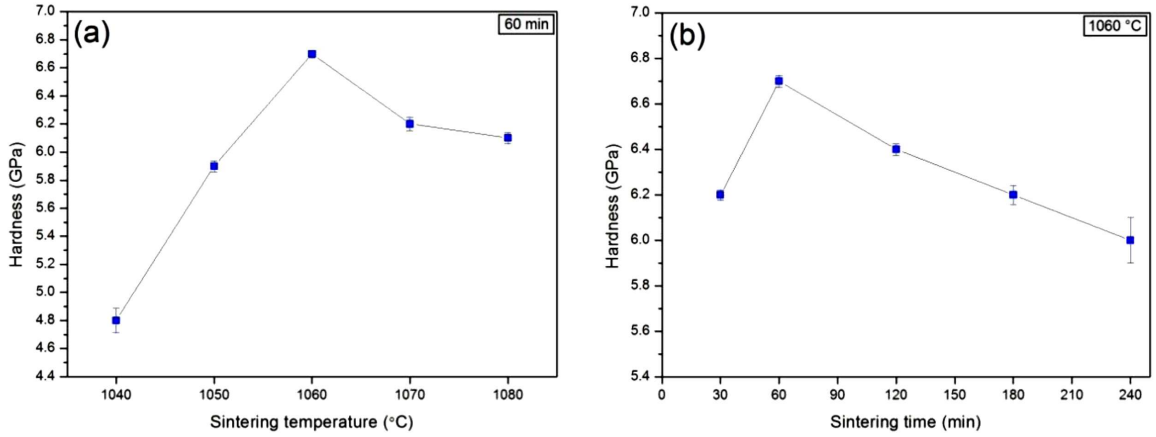

Figure 11. Hardness of ceramic samples attained after sintering of the andesite basalt powder at: a) different temperatures for 60 min and b) 1060 °C for different sintering time (variability of the measured hardness values is presented with standard deviation)

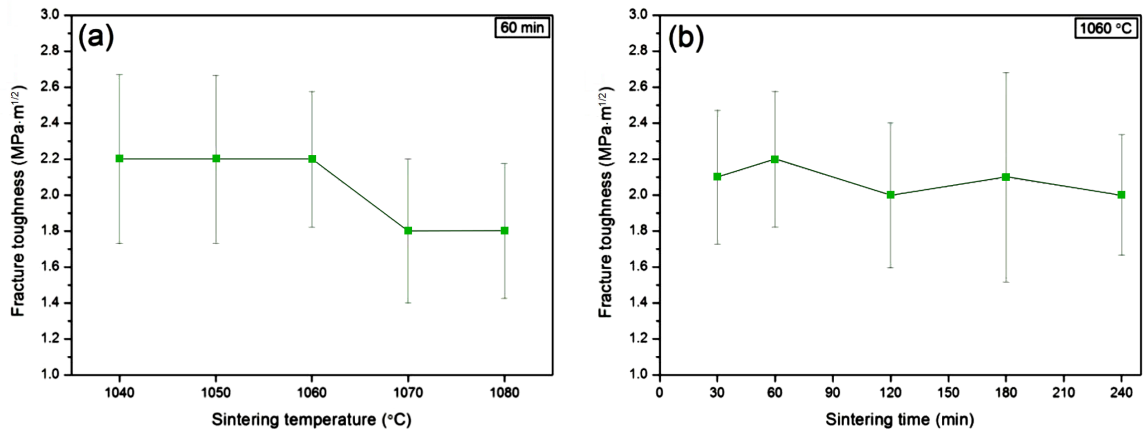

Figure 12. Fracture toughness of ceramic samples attained after sintering of the andesite basalt powder at: a) different temperatures for 60 min and b) 1060 °C for different sintering time (variability of the measured fracture toughness values is presented with standard deviation)

sity values (Fig. 5) and the measured hardness values (Fig. 11a), the expected conclusion can be drawn that the hardness correlates with density of the sintered samples and with an increase of the sample relative density, its hardness increases accordingly.

The effect of sintering time on the hardness of the ceramic samples attained during sintering of the andesite basalt powder at 1060 °C is presented in Fig. 11b. It is clear that a decrease in sintering time to 30 min, as well as an increase in sintering time to 120, 180 and 240 min, did not contribute to an increase of the hardness value. Namely, when the sintering duration increases from 60 to 240 min, the hardness decreases linearly due to a decrease in the sintered ceramic samples density. The maximal hardness value of 6.7 GPa was attained at the optimal sintering temperature during sintering for 60 min.

The effect of sintering temperature on the fracture toughness of the ceramic samples attained during sintering of the andesite basalt powder for 60 min is presented in Fig. 12a. Results obtained during the present study show that the fracture toughness value remains unchanged when sintering temperature is increased from 1040 to 1060 °C and reaches a value of 2.2 MPa·m$^{1/2}$. However, a further increase of sintering temperature to 1070 and 1080 °C induced a decrease of the fracture toughness to 1.8 MPa·m$^{1/2}$.

The effect of sintering time on the fracture toughness of ceramic samples attained after sintering of the andesite basalt powder at 1060 °C is shown in Fig. 12b. Presented results show that at the optimal sintering temperature the fracture toughness values vary only slightly in the narrow range from 2.0 to 2.2 MPa·m$^{1/2}$ even though the sintering duration is changed in the experiments by 5 times (from 30 to 240 min). The maximal fracture toughness value of 2.2 MPa·m$^{1/2}$ was reached after sintering for 60 min, while the minimum value of 2.0 MPa·m$^{1/2}$ was reached after sintering for 240 min. From the results presented in Fig. 12b it is clear that a longer sintering time at the optimal sintering temperature of 1060 °C did not contribute to an increase in the fracture toughness, although this could be expected as this is the case with most ceramic materials.

Figure 13 shows the impression of a square-based diamond pyramid made at the surface of the high-density ceramic sample sintered under the optimal sintering conditions, i.e. at 1060 °C for 60 min, for which the highest relative density of 99.5% was obtained and cracks created at the corners of the impression made during the Vickers test method. It can be seen that the crack propagation is radial relative to the axis of the imprint and that formed cracks have not branched out into many smaller cracks.

If the maximal fracture toughness value of 2.20 MPa·m$^{1/2}$, obtained during this study, is compared with the fracture toughness values of some aluminosilicate rocks, such as granite (granite fracture toughness value is ranging from 0.97 to 1.15 MPa·m$^{1/2}$) [40], it can be concluded that during this study the

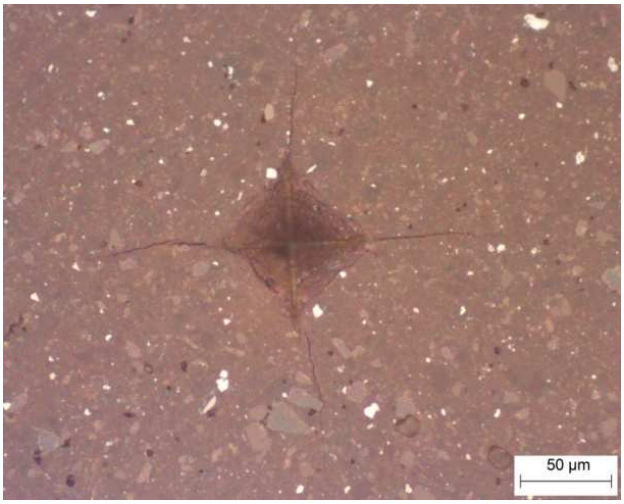

Figure 13. LOM micrograph showing the Vickers indentation impression and cracks formed at the surface of the ceramic sample attained after sintering of the andesite basalt powder at 1060 °C for 60 min

optimization of the sintering procedure led to the fabrication of the refractory high-density ceramics with the fracture toughness value two times higher than granite.

IV. Conclusions

Raised public awareness on the usage of green technological solutions in the industrial practice focused the presented research on the development of low-cost procedures in order to obtain high-density ceramics with multiple applications by using the abundant environmentally-friendly raw materials, such as andesite basalt. The present research was aimed at the obtaining and optimization of the technological process for the production of refractory high-density ceramics using the andesite basalt from the deposit site "Donje Jarinje", Serbia, as the starting raw material and resulting conclusions are summarized as follows:

1. XRD analysis showed that phase transformations did not occur during the andesite basalt sintering in the investigated temperature range from 1040 to 1080 °C. However, when XRD patterns of the obtained ceramic materials were compared with XRD pattern of starting andesite basalt powder the appearance of reddish-brown haematite become apparent due to the sintering procedure conducted in the air.
2. Sintering in air was successfully applied to obtain the high-density ceramics by using the andesite basalt rock as a low-cost raw material. Relative density of 99.5% was achieved for the ceramic samples produced through the optimized technological process that included the obtaining of bimodal andesite basalt powder and sintering at 1060 °C for 60 min. Application of these optimized sintering parameters ensured the attainment of the basalt-based ceramics with the highest relative density compared to the results available in the relevant literature.
3. The highest shrinkage of 12.81% was achieved for the high-density ceramics during the sintering at an optimal temperature of 1060 °C for 60 min.
4. During sintering in air, no significant loss of material was detected.
5. The highest hardness and fracture toughness values of 6.7 GPa and 2.2 MPa·m$^{1/2}$, respectively, were achieved during the sintering at 1060 °C for 60 min.

Results of the presented study demonstrated that the andesite basalt can be successfully used for the production of high-density ceramics with satisfactory mechanical properties suitable for various industrial applications. The high-density ceramics obtained by sintering of andesite basalt can be used to make tiles for floor and wall surfaces in the civil engineering. The application of andesite basalt ceramics is based on its excellent chemical resistance, good thermal stability, low thermal conductivity and relatively high hardness and fracture toughness. Also, the obtained high-density ceramics can be used as a matrix in the production of advanced composite materials.

Acknowledgements: This work was financially supported by the Ministry of Education, Science, and Technological Development of the Republic of Serbia (Contract No. 451-03-9/2021-14/200017). Authors would also like to acknowledge the help of Dr. Smilja Marković from the Institute of Technical Sciences of The Serbian Academy of Sciences and Arts (SASA), Serbia, during the particle size distribution analysis.

References

1. S.A. Morse, *Basalts and Phase Diagrams: An Introduction to the Quantitative Use of Phase Diagrams in Igneous Petrology*, Springer-Verlag, New York (US) 1980.
2. A.I. Poznyak, I.A. Levitskii, S.E. Barantseva, "Basaltic and granitic rocks as components of ceramic mixes for interior wall tiles", *Glas. Ceram.*, **69** [7-8] (2012) 262–266.
3. S. Kapur, N. Sakarya, C. Karaman, E.A. Fitzpatrick, M. Pagliai, "Micromorphology of basaltic ceramics", *Brit. Ceram. Trans.*, **94** [1] (1995) 33–37.
4. M. Kirsch, G. Berger, U. Banach, T. Hubert, "Vitroceramics - A non-conventional kind of ceramics", *Intercer.*, **37** [3] (1988) 34–38.
5. B. Matović, S. Bošković, M. Logar, "Preparation of basalt-based glass ceramics", *J. Serb. Chem. Soc.*, **68** [6] (2003) 505–510.
6. D. Čikara, A. Todić, T. Todić, "Istraživanje mogućnosti primene domaćih bazalta za proizvodnju bazaltnog stakla", *IMK 14 - Istraživanje i razvoj*, **16** [4] (2010) 1–5 (in Serbian).
7. B. Wei, H. Cao, S. Song, "Environmental resistance and mechanical performance of basalt and glass fibers", *Mater. Sci. Eng. A. - Struct.*, **527** (2010) 4708–4715.
8. A. Todić, D. Čikara, T. Todić, B. Ćirković, "Ispitivanje žilavosti čestičnog kompozita na bazi bazalta polimera i silana", *IMK 14 - Istraživanje i razvoj*, **15** [3-4] (2009) 25–28 (in Serbian).
9. G.A. Khater, M.O. Abu Safiah, E.M.A. Hamzawy, "Augite-anorthite glass-ceramics from residues of basalt quarry and ceramic wastes", *Process. Appl. Ceram.*, **9** [2] (2015) 117–123.
10. S. Matkó, S. Keszei, I. Csontos, P. Anna, G. Marosi, M. Zsuga, J. Borda, G. Nagy, "Fire retarded insulating sheets from recycled materials", *Macromol. Symp.*, **233** (2006) 217–224.
11. M.C. Wang, Z.G. Zhang, Y.B. Li, "Chemical durability and mechanical properties of alkali-proof basalt fiber and its reinforced epoxy composites", *J. Reinf. Plast. Comp.*, **27** [4] (2008) 393–407.
12. A. Prstić, R. Simić, Lj. Andrić, Z. Aćimović, "Melting and casting of basalt ore", pp. 893–897 in *X Balkan Mineral Processing Congress: Mineral Processing in 21st Century*, Varna, 2003.
13. A. Prstić, Z. Aćimović-Pavlović, Lj. Andrić, M. Ćosić, Z. Aćimović, "Application of casting materials based on basalt ore in metallurgy and mining industry", pp. 422–425 in *XI Balkan Mineral Processing Congress: Mineral Processing in Sustainable Development*, Tirana, 2005.
14. G.H. Beall, H.L. Rittler, "Basalt glass ceramics", *Am. Ceram. Soc. Bull.*, **55** [6] (1976) 579–582.
15. M. Pavlović, M. Sarvan, F. Klisura, Z. Aćimović, "Basalt - raw material for production of aggregate for modern road

and rail shourd", pp. 175–183 in *4th Conference Maintenance*, Zenica, 2016.
16. M. Pavlović, M. Duricic, A. Mumdic, "Basalt application prospects for touristic facilities furnishing", pp. 53–60 in *Conference SED*, Užice, 2015.
17. D. Čikara, A. Todić, D. Čikara-Anić, "Possibilities of production of wear resistant construction elements by processing of Serbian basalt", *FME Trans.*, **38** [4] (2010) 203–207.
18. Lj. Andrić, Z. Aćimović-Pavlović, M. Trumić, A. Prstić, Z. Tanasković, "Specific characteristic of coating glazes based on basalt", *Mater. Des.*, **39** (2012) 9–13.
19. L.F. Lima, P.Q. Mantas, A.M. Segadães, R.C.D. Cruz, "Processing and characterization of sinter-crystallized basalt glass-ceramics", *J. Non-Cryst. Solids*, **538** (2020) 120019.
20. L.F. Lima, J.E. Zorzi, R.C.D. Cruz, "Basaltic glass-ceramic: A short review", *Bol. Soc. Esp. Ceram. V.*, **61** [1] (2020) 2–12.
21. G.A. Khater, M.A. Mahmoud, "Preparation and characterization of nucleated glass-ceramics based on basaltic rocks", *J. Austral. Ceram. Soc.*, **53** (2017) 433–441.
22. G.A. Khater, A. Abdel-Motelib, A.W. El Manawi, M.O. Abu Safiah, "Glass-ceramics materials from basaltic rocks and some industrial waste", *J. Non-Cryst. Solids.*, **358** [8] (2012) 1128–1134.
23. J.M. Klein, K.M.S. da Silva, A.P. Titton, R.C.D. Cruz, C.A. Perottoni, J.E. Zorzi, "Microstructure and mechanical properties of a nucleant-free basaltic glass-ceramic", *Mater. Sci. Technol.*, **35** [5] (2019) 544–551.
24. M. Cocić, M. Logar, B. Matović, V. Poharc-Logar, "Glass-ceramics obtained by the crystallization of basalt", *Sci. Sinter.*, **42** [3] (2010) 383–388.
25. H. Jamshaid, R. Mishra, "A green material from rock: basalt fiber – A review", *J. Text. I.*, **107** [7] (2016) 923–937.
26. E. Albert, M. Muntean, A. Ianculescu, F. Miculescu, B. Albert, "Special ceramic material based on basaltic-andesite for extreme environments", *Adv. Mater. Res.*, **59** (2009) 39–41.
27. B. Matovic, J. Maletaskic, J. Zagorac, V. Pavkov, R.S.S. Maki, K. Yoshida, T. Yano, "Synthesis and characterization of pyrochlore lanthanide (Pr,Sm) zirconate ceramics", *J. Eur. Ceram. Soc.*, **40** [7] (2020) 2652–2657.
28. A.G. Evans, E.A. Charles, "Fracture toughness determinations by indentation", *J. Am. Ceram. Soc.*, **59** [7-8] (1976) 371–372.
29. C.B. Ponton, R.D. Rawlings, "Vickers indentation fracture toughness test Part 1: Review of literature and formulation of standardized indentation toughness equations", *Mater. Sci. Technol.*, **5** [9] (1989) 865–872.
30. C.B. Ponton, R.D. Rawlings, "Vickers indentation fracture toughness test Part 2: Application and critical evaluation of standardized indentation toughness equations", *Mater. Sci. Technol.*, **5** [10] (1989) 961–976.
31. J.C. Glandus, T. Rouxel, Q. Tai, "Study of the Y-TZP toughness by an indentation method", *Ceram. Int.*, **17** [2] (1991) 129–135.
32. A. Karamanov, S. Ergul, M. Akyildiz, M. Pelino, "Sinter-crystallization of a glass obtained from basaltic tuffs", *J. Non-Cryst. Solids*, **354** [2-9] (2008) 290–295.
33. A. Karamanov, L. Maccarini Schabbach, E. Karamanova, F. Andreola, L. Barbieri, B. Ranguelov, G. Avdeev, I. Lancellotti, "Sinter-crystallization in air and inert atmospheres of a glass from pre-treated municipal solid waste bottom ashes", *J. Non-Cryst. Solids*, **389** (2014) 50–59.
34. A. Karamanov, G. Taglieri, M. Pelino, "Sintering in nitrogen atmosphere of iron-rich glass-ceramics", *J. Am. Ceram. Soc.*, **87** [7] (2004) 1354–1357.
35. A. Karamanov, "Vitrification and sinter-crystallization of iron-rich industrial wastes", *Adv. Sci. Technol.*, **92** (2014) 174–183.
36. S.V. Fomichev, N.P. Dergacheva, A.V. Steblevskii, V.A. Krenev, "Production of ceramic materials by the sintering of ground basalt", *Theor. Found. Chem. Eng.*, **45** [4] (2011) 526–529.
37. A. Karamanov, L. Arrizza, S. Ergul, "Sintered material from alkaline basaltic tuffs", *J. Eur. Ceram. Soc.*, **29** [4] (2009) 595–601.
38. M. Abass, Y. Kanda, "Ceramics based on concrete wastes prepared by spark plasma sintering", *Process. Appl. Ceram.*, **15** [1] (2021) 100–109.
39. N.F. Drobot, O.A. Noskova, A.V. Khoroshilov, A.V. Steblevskii, S.V. Fomichev, V.A. Krenev, "Effect of iron content on the sintering of ground basalt into ceramics", *Inorg. Mater.*, **50** (2014) 314–319.
40. S.S. Jeong, K. Nakamura, S. Yoshioka, Y. Obara, M. Kataoka, "Fracture toughness of granite measured using micro to macro scale specimens", *Procedia Eng.*, **191** (2017) 761–767.